Polythiophene-Fullerene Based Photodetectors: Tuning of Spectral Response and Application in Photoluminescence Based (Bio)Chemical Sensors

By *Kanwar S. Nalwa, Yuankun Cai, Aaron L. Thoeming, Joseph Shinar, Ruth Shinar,** and *Sumit Chaudhary**

Organic electronics is attracting extensive interest for the development of low-cost and flexible devices, such as solar cells,[1] light-emitting diodes (LEDs),[2] and photodetectors.[3] Recently, the use of organic electronics has been broadened toward novel devices, including photoluminescence (PL)-based (bio)chemical sensors using organic LEDs (OLEDs) as excitation sources.[4] The viability of a (bio)chemical sensing platform increases when the fabrication of all its components is simple, and they are compact and easily integratable. In this direction, an integrated platform based on OLED pixel excitation, a luminescing sensing medium, and PL-detecting organic photodetectors (OPDs) is a promising approach. This communication describes steps toward the development of such a compact sensing platform. In particular, a bulk-heterojunction OPD based on poly(3-hexylthiophene) and fullerene derivatives was engineered to be sensitive to the sensing film's PL, with a fast response time for monitoring analytes in both the PL intensity and PL decay time detection modes.

The need for (bio)chemical sensing systems is burgeoning for various analytical problems in fields such as medicine, the environment, defense and food. Optical sensing techniques – most notably luminescence-based – are sometimes the only ones that provide adequate sensitivity.[5] In general, luminescence-based (bio)chemical sensors require three components (excluding the electronics and readout): a fluorescing or phosphorescing sensing element, a light source that excites the PL of that sensing element, and a photodetector. Traditional light sources are lasers or LEDs that cannot be easily integrated with the other components due to size, geometrical, or operational constraints.[6] Traditional photodetection elements include charge coupled device cameras, photomultiplier tubes, and inorganic photodiodes, which are also hampered by integrability issues. In the past few years, Shinar et al. have demonstrated the efficacy of the OLED-based platform for PL-based sensing of various analytes.[7–13] We believe that integration of organic photodetectors (OPDs) with this – hence an all-organic sensing platform – has the potential to truly enable the development of flexible, thin, miniature sensor arrays via a facile and low-cost fabrication route. There have been only a few reports on the use of OPDs in PL-based sensors. Kraker et al.[14] recently reported a solid-state OLED/dye/OPD sensing system for PL intensity-based detection, requiring polarization filters to prevent the OLED's electroluminescence (EL) from reaching the OPD. Such EL blocking is crucial for the intensity-based detection methodology. Hofmann et al.[5] reported the use of an OPD to monitor a chemiluminescent reaction in a microfluidic system. Here, we report for the first time, the exploration of an OLED/dye/OPD-based sensing system in both PL intensity (I) and decay time (τ) detection modes. The τ mode is preferable as it eliminates the need for (i) frequent sensor calibration, since τ is insensitive to small changes in I, minor film degradation, or background light[9,15,16] and (ii) optical filters, as τ is monitored during the off period of the pulsed excitation.

We explored poly(3-hexylthiophene): [6,6]-phenyl-C61-butyric acid methyl ester (P3HT:PCBM)-based bulk-heterojunction type devices as our OPDs due to their solution processibility and superior performance in the area of photovoltaics.[17,18] For quantitation of our OPD's response, oxygen and glucose were chosen as the analytes. The sensing element usually contains an oxygen-sensitive dyes, such as Pt or Pd octaethylporphyrin (PtOEP or PdOEP, respectively).[7–13] The collisions of the dye molecules with O_2 decrease I and τ.[9,15,16] Ideally, in a homogeneous matrix, the O_2 concentration can be determined by monitoring τ or the steady-state I using the Stern–Volmer (SV) equation[19]

$$I_o/I = \tau_o/\tau = 1 + K_{SV}[O_2] \quad (1)$$

where I_o and τ_o are the unquenched values and K_{SV} is a constant. We used PtOEP in our experiments. It was embedded in a TiO_2 nanoparticle-doped polystyrene film. TiO_2 improves EL absorption by PtOEP by increasing scattering within the polystyrene matrix.[11] Both inorganic LEDs and small-molecule OLEDs were utilized as green excitation sources (emission peak ~525 nm). The LEDs were operated in a pulsed mode (100 μs pulse width at 50 Hz). The PL of the sensing film is in the red region (~640 nm). Hence, as a first step, the processing of the P3HT:PCBM active layer was tailored to improve the photoresponse of these OPDs in the red, which otherwise peaks in the green and is weak in the red.[17,18]

[*] K. S. Nalwa, A. L. Thoeming, Prof. J. Shinar, Prof. R. Shinar, Prof. S. Chaudhary
Department of Electrical and Computer Engineering and Microelectronics Research Center
Iowa State University
Ames, IA 50011 (USA)
E-mail: rshinar@iastate.edu; sumitc@iastate.edu
Dr. Y. Cai, Prof. J. Shinar
Ames Laboratory-USDOE
& Department of Physics and Astronomy
Iowa State University
Ames, IA 50011 (USA)

DOI: 10.1002/adma.201000417

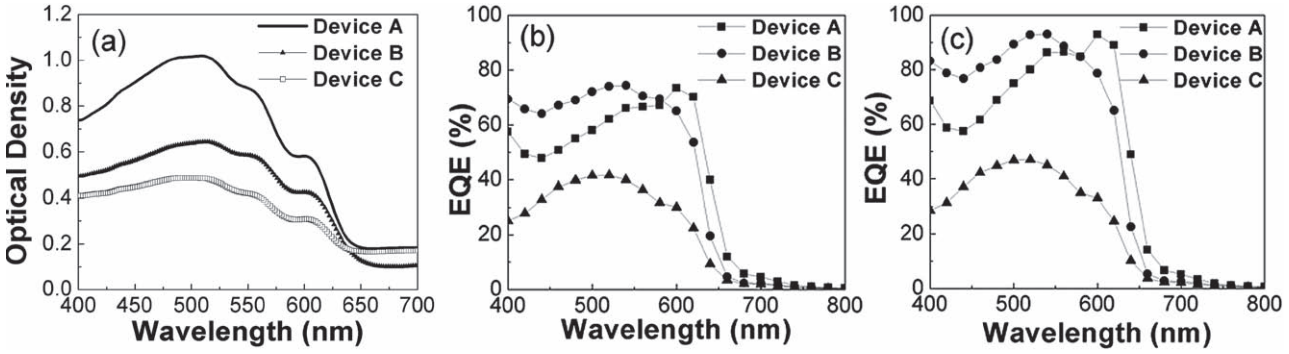

Figure 1. Effect of active layer growth conditions. a) UV-vis absorption spectra for films of P3HT/PCBM (1:1 wt/wt ratio), spin-coated at 400 rpm for 30 seconds – Device A, 600 rpm for 60 seconds – Device B, and 1000 rpm for 60 seconds – Device C. b) EQE spectra of devices A, B, and C at short circuit; and c) at 0.5 V reverse bias.

In an effort to red-shift the EQE spectrum, three types of OPDs (A, B, and C) with different active layer thicknesses were obtained by spin-coating at 400, 600, and 1000 rpm for 30, 60, and 60 s, respectively (see supporting information for device schematic). The absorption spectra of these P3HT:PCBM layers are shown in **Figure 1a**. Device A, because its active layer is thicker (~350 nm) than those of devices B (~220 nm) and C (~140 nm), demonstrates the highest absorption at all wavelengths. The three absorption shoulders are more pronounced in device A, indicating a higher degree of self-organization of P3HT chains arising from the slowest drying rate, due to the lower spin speed and duration.[17] This self-organization leads to high crystalline order involving an enhanced conjugation length of P3HT chains.[17,20] The EQE spectra for the three devices were measured in short-circuit condition (Figure 1b), and at 0.5 V reverse bias (Figure 1c). The EQE at short circuit condition for device A shows a maximum of ~70% at 600 nm, while the peak is at 540 nm (EQE ~70%) for device B, and 520 nm (EQE ~40%) for device C. The thinner films' thickness (devices B and C) is less than the penetration depth of the strongly absorbed green light, so that the green photons can create a uniform distribution of photogenerated carriers throughout the thickness. But for the thicker film (device A), green photons, having a high absorption coefficient, are absorbed closer to the anode. This makes the electrons more susceptible to recombination, as they have to travel the entire active layer thickness to reach the Al electrode. In contrast, the red photons can penetrate greater thickness to generate a more uniform carrier distribution. Hence, for device A, the collection efficiency of charge carriers created by red photons is higher than that created by green photons, which explains the 600 nm EQE peak. The EQE dependence on wavelength does not change with 0.5 V reverse bias. However, collection at every wavelength improves, enhancing the overall EQE. At PtOEP's emission peak of 640 nm, device A showed the highest EQE of ~40% at 0 V and ~50% at –0.5 V. In general, photodetectors can be operated at either zero or reverse bias. Operation at zero bias is however advantageous in one aspect, that is, lower dark current which assures a high dynamic range. For device A, the dark current was less than 1 nA/cm^2, leading to a dynamic range exceeding 10^7 (see Supporting Information).

To elucidate the structural properties of the P3HT:PCBM films, atomic force microscopy (AFM) was employed. Height AFM images (**Figure 2**) show that the surface r.m.s. roughness values, σ, for films A and B are 10.7 and 7.2 nm, respectively. For film C, the smoothest surface, with $\sigma \sim 1.05$ nm, is observed. The high surface roughness of slowly spin-coated films A and B is another signature of polymer (blend) self-organization, and can be correlated to formation of nanocrystallites due to ordering and stacking of P3HT supermolecules.[17] Raman spectra also show narrowing of the peak related to –C=C– symmetric stretching in the active layer of device A, which indicates higher P3HT crystallinity (see Supporting Information).[21–24] Higher P3HT crystallinity involves enhanced conjugation length, which leads to enhanced absorption in the red. This, in

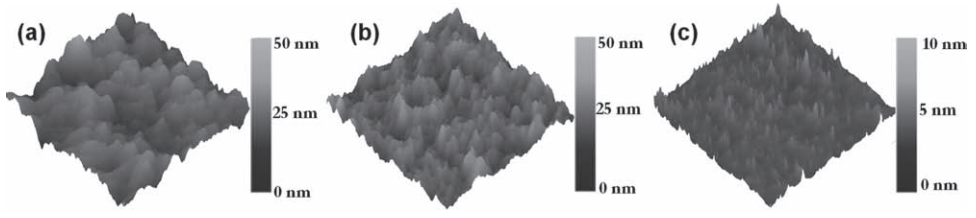

Figure 2. AFM height images of the P3HT/PCBM composite films (PCBM concentration = 50 wt%) showing the active layer of (a) device A (b) device B and (c) device C. Scan area is 5 μm × 5 μm in all cases. Note that the color scale for films A and B is 0–50 nm, whereas for film C it is 0–10 nm.

addition to greater film thickness, can also be partially responsible for enhanced red EQE in device A.

Due to enhanced EQE in the red, device A was chosen as the OPD for our sensors. The OPD, assembled with the sensing film and a 600 nm long-pass filter, was first tested for O_2 sensing using the inorganic LED with peak emission at ~525 nm. In another experiment, an OLED was used. As a first step towards structural integration, the LED, PS:PtOEP sensing film, long pass filter, and P3HT:PCBM OPD were assembled in the front detection geometry (see supporting information for schematic). The filter was placed between the OPD and the sensing film to prevent the green EL from reaching the OPD. Note that the filter is required only for the *I* detection mode. The τ mode does not require it, since measurements are done following the excitation pulse, i.e. in the (O)LED's off state.

Figure 3 shows the OPD response to the sensor's PL following the LED excitation pulse and exposure to different concentrations of O_2 in Argon. As expected, *I* and τ decrease with increasing O_2 concentration due to collisional quenching, to which the OPD responds with a reduced photocurrent and its faster decay. This PL quenching of PtOEP by O_2 is due to the paramagnetic triplet nature of ground state O_2 and singlet nature of excited O_2,[16] which is unique among common gases. Figure 3b shows I_o/I (I_o is the intensity in 100% Ar) versus the gas-phase O_2 concentration. The dependence was found to be linear with O_2 concentration up to 40% O_2, with signal ratio $S \equiv I_o/I$ (40% O_2) ~ 10, which can be further improved by using a 630 nm long-pass filter. The SV curve for the τ mode shows that τ_o/τ for 20% oxygen is 2.5, which is lower than the *I* mode ratio. However, other advantages associated with the τ mode, as discussed earlier, make it more viable for practical applications. The deviation of the τ mode SV plot from linearity probably arises from inhomogeneity in the dye's environment, i.e. the dye molecules occupy quencher-easy accessible and quencher-difficult accessible sites,[25] which leads to different contributions to PL quenching. However, the exact mechanism is not clear at this point.

Glucose sensing using the LED/PS:PtOEP sensing element/P3HT:PCBM OPD configuration relied on the enzymatic oxidation of glucose by glucose oxidase (GO_x) and oxygen. In the presence of glucose and GO_x, the PL quenching of the dye molecules is reduced due to consumption of dissolved oxygen (DO). The DO's initial concentration ($[DO]_{initial}$) in water is ~0.26 mM at room temperature. For a concentration of the active isomer of glucose ($[\beta\text{-D-glucose}]_{initial} < [DO]_{initial}$, at the completion of the oxidation reaction, $[\beta\text{-D-glucose}]_{initial}$ equals the difference between the initial and final DO levels. With increased $[\beta\text{-D-glucose}]_{initial}$, the residual DO decreases, hence the *I* and τ of PtOEP increase (Figure 3c,d). Integration under the PL τ curve, corresponding to each $[\beta\text{-D-glucose}]_{initial}$, was used to represent the *I*. It can be seen that $1/I$ is linear with $[\beta\text{-D-glucose}]_{initial}$, which is expected from a modified SV equation.[12] The τ mode curves slightly deviate from linearity similar to the case of the gas-phase O_2.

Finally, following the demonstration of the suitability of the OPD for O_2 and glucose sensing, including in the τ mode, the inorganic LED was replaced by an OLED to demonstrate the viability of an all-organic sensor platform. In this experiment, *I* and τ clearly decrease as the O_2 concentration is increased, as expected (Figure 3e,f). The observed higher noise in the photocurrent decay curves is due to instabilities in the EL and lower brightness than the inorganic LED. I_o/I is linear with O_2

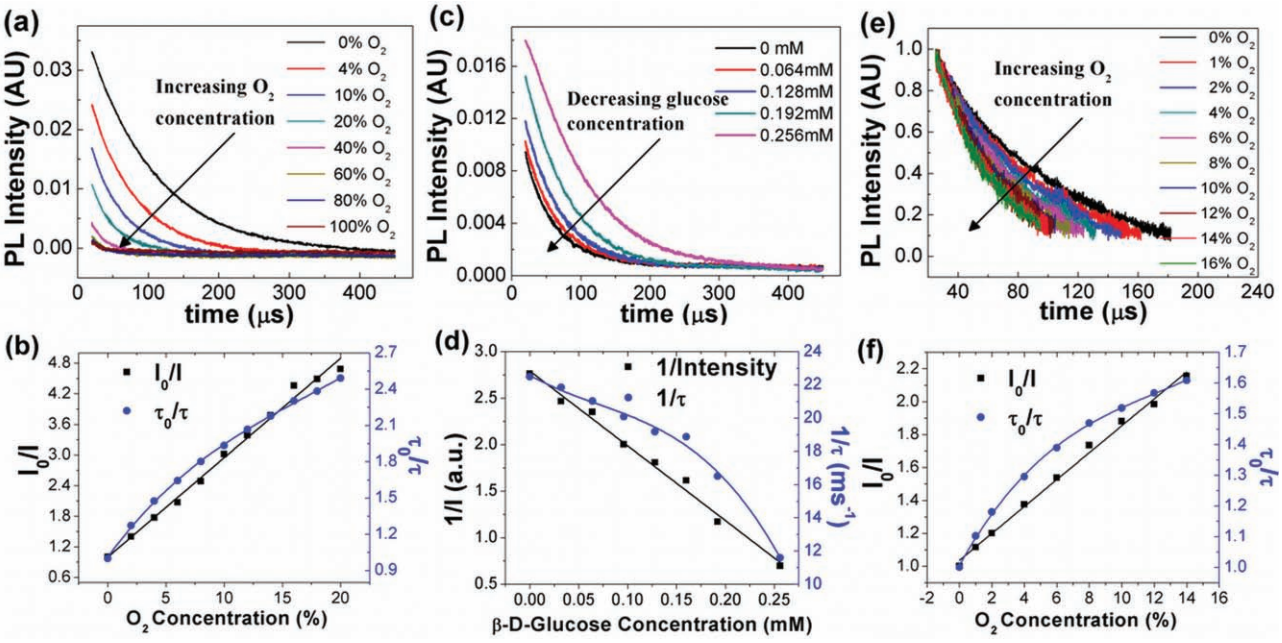

Figure 3. The effect of concentration of gas-phase O_2 (a) and glucose (c) on the OPD's temporal photocurrent response. Excitation source was an LED. (b) and (d) are *I* and τ-based SV calibration curves corresponding to (a) and (c), respectively. For OLED excited O_2 sensor, (e) and (f) show the effect of O_2 concentration on the OPD temporal response and corresponding SV calibration curves, respectively.

concentration and the ratio I_o/I for 15% oxygen is 2.1. Although this ratio should be the same whether using an LED or OLED, it has previously been shown that weaker excitation by the OLED generally results in a lower ratio.[10,13] The results with the OLEDs can therefore be improved by utilizing brighter (and encapsulated) OLEDs. The ratio τ_o/τ for 15% oxygen is 1.6 and is comparable to the value observed when using the inorganic LED, since performance in the τ mode is independent of the intensity of excitation source.

In summary, a structurally integrated all organic sensing platform – OLED pixels exciting a luminescent dye; the dye's PL intensity and decay-time depending on an analyte's concentration; and these PL changes of the dye being detected by OPDs – is a promising approach to achieve low-cost, flexible and compact sensor arrays. This communication presented steps towards realizing this paradigm in one of the several possible embodiments – a front detection geometry, wherein, the (O)LED, the dye embedded film, and the OPD were spatially assembled in the same order. We engineered the P3HT:PCBM OPDs to tailor their photoresponse towards the red emitting dye (PtOEP) based O_2 and glucose sensors. Devices realized from a thicker and slower-grown P3HT:PCBM layer showed the highest EQE of 40% without bias at 640 nm, which is the peak emission of the sensing dye. Oxygen and glucose concentrations were monitored using the optimized OPD via detection of the dye's I or τ. The latter eliminates the need for frequent sensor calibration or optical filters. The response of the OPDs was sufficiently fast to monitor the O_2 using the τ mode. Finally, after demonstrating the efficacy of OPDs with inorganic LEDs, this report also demonstrated all-organic O_2 sensors, which, in addition to OPDs, used OLEDs as the light source.

Experimental Section

OPD fabrication and characterization: For OPD fabrication, a conducting film of poly(3,4-ethylenedioxythiophene) doped with poly(styrenesulfonate) (PEDOT:PSS, Clevios P) was spin coated at 3000 rpm after UV-Ozone plasma exposure of cleaned ITO-coated slides, followed by annealing at 120 °C for 5 min. The P3HT:PCBM blend solution (17 mg/mL in dichlorobenzene) was spin coated at different speeds. An Al (100 nm) electrode was deposited by thermal evaporation on top of the active layer. The absorption spectra were measured by a Varian Cary 5000 UV-vis-NIR spectrophotometer. EQE measurements were done using ELH Quartzline lamp (120 V–300 W from GE) and a monochromator with a lock-in amplifier to eliminate background noise. The reference was a calibrated Si photodiode with known EQE spectra. The P3HT:PCBM layer thicknesses were obtained by forming a 100 µm wide scratch on the films using a fine blade. AFM (Veeco Nanoscope III) tip in tapping mode was scanned across the scratch to find the thickness of the P3HT:PCBM films. Raman spectra were recorded on a Renishaw inVia Raman microscope equipped with a low noise and high sensitivity RenCam CCD detector, and a 488 nm, 0.3 mW laser. The reflected Raman signal was collected using a 50X objective with a numerical aperture of 0.7. The signal collection time was 10 s and the scan was averaged twice. To mimic the device fabrication conditions, all the films for absorption and Raman spectra measurement were spun cast on PEDOT:PSS-covered ITO-coated glass substrates.

OLED Fabrication: 20 Ω/ ITO/glass was obtained from Colorado Concept Coatings. Copper phthalocyanine (CuPc) and LiF were obtained from Sigma-Aldrich. N,N′-diphenyl-N,N′-bis(1-naphthyl phenyl)-1,1′-biphenyl-4,4′-diamine (NPD), 2,3,6,7-Tetrahydro-1,1,7,7,-tetramethyl-1H,5H,11H-10-(2- benzothiazolyl) quinolizino-[9,9a,1gh] coumarin (C545T), and tris(8-hydroxyquinoline) Al (Alq_3) were obtained from H.W. Sands. Green emitting (peaking at ~525 nm) OLED pixels were fabricated by thermally evaporating organic materials on top of ~150 nm thick cleaned and UV ozone-treated ITO-coated glass. The organic layers, in sequence, are the hole injection layer ~5 nm CuPC, hole transport layer ~50 nm NPD, doped emitting layer ~20 nm C545T:Alq_3 (1% w/w), and electron transport layer ~30 nm Alq_3, which is followed by an electron injection layer ~1 nm LiF and the ~100 nm Al cathode. OLED pixels were generated by etching the ITO into two 2 mm wide strips; the OLED pixels are defined by the overlapping regions of mutually perpendicular ITO and Al strips. Two OLED pixels (2 mm × 2 mm) were used as the excitation source for the PL measurements.

Sensing Experiment: PS:PtOEP sensor films were prepared by drop casting 50 µL of a toluene solution with 1 mg/mL PtOEP, 1 mg/mL TiO_2 and 40 mg/mL polystyrene. The films were dried in the dark at ambient temperature. GOx from *Aspergillus niger* was obtained from Sigma-Aldrich. GOx and glucose (Fisher Scientific) were dissolved in phosphate buffer (PH 7.4), at the desired concentrations. The sensor components – an LED, PS:PtOEP sensing film, long-pass filter, and P3HT:PCBM OPD – were assembled in a front detection mode, where the sensing film is sandwiched between the OPD and LED. For O_2 sensing experiments, the sensor film was enclosed in a flow cell through which different volumetric ratios of Ar/O_2 gas mixture were passed. The inorganic LEDs were operated in a pulsed mode at a bias of 3.7 V, pulse width of 100 µs, and a repetition rate of 50 Hz. The photocurrent signal from the OPD at zero bias was amplified using a gain of 10^6 V/A at 200 kHz bandwidth, and monitored on an oscilloscope. The PL lifetimes were obtained by monitoring the OPD response following the application of the LED pulse. For glucose sensing, a glass tube was glued on top of the sensor film, forming a reaction well (200 µL in volume), enclosing the dye-coated film at the bottom. 100 µL of glucose and GO_x were sequentially added into the reaction well, followed by hermetic sealing using a cover glass. The PL signal was collected by the OPD after 1 minute of adding the solutions. The concentration of GO_x (300 units/mL) was sufficient to catalyze glucose oxidation in the range of 0 to 0.3 mM, depleting the DO in 20 s.

Supporting Information

Supporting Information is available from the Wiley Online Library or from the author.

Acknowledgements

SC, KSN, and AL thank the Institute of Physical Research and Technology, Iowa State University for Company Assistance grant. SC, RS, and JS thank the Iowa Power Fund. JS and YC thank the Ames Laboratory, which is operated by Iowa State University for the US Department of Energy (USDOE) under Contract No. DE-AC 02–07CH11358. The work was partially supported by the Director for Energy Research, Office of Basic Energy Sciences, USDOE. RS and Integrated Sensor Technologies thank NSF for an SBIR Phase II grant.

Received: February 4, 2010
Published online: August 30, 2010

[1] H-Y. Chen, J. Hou, S. Zhang, Y. Liang, G. Yang, Y. Yang, L. Yu, Y. Wu, G. Li, *Nat. Photon.* **2009**, *3*, 649.
[2] K. M. Vaeth, *Inform. Display* **2003**, *19*, 12.
[3] X. Gong, M. Tong, Y. Xia, W. Cai, J. S. Moon, Y. Cao, G. Yu, C-L. Shieh, B. Nilsson, A. J. Heeger, *Science* **2009**, *325*, 1665.
[4] J. Shinar, R. Shinar, *J. Phys. D: Appl. Phys.* **2008**, *41*, 133001.
[5] O. Hofmann, X. Wang, A. Cornwell, S. Beecher, A. Raja, D. D. C. Bradley, A. J. deMello, J. C. deMello, *Lab Chip* **2006**, *6*, 981.

[6] E. J. Cho, F. V. Bright, *Anal. Chem.* **2001**, *73*, 3289.
[7] V. Savvate'ev, Z. Chen-Esterlit, J. W. Aylott, B. Choudhury, C. H. Kim, L. Zou, J. H. Friedl, R. Shinar, J. Shinar, R. Kopelman, *Appl. Phys. Lett.* **2002**, *81*, 4652.
[8] B. Choudhury, R. Shinar, J. Shinar, *J. Appl. Phys.* **2004**, *96*, 2949.
[9] R. Shinar, Z. Zhou, B. Choudhury, J. Shinar, *Anal. Chim. Acta* **2006**, *568*, 190.
[10] R. Shinar, D. Ghosh, B. Choudhury, M. Noack, V. L. Dalal, J. Shinar, *J. Non-Cryst. Solids* **2006**, *352*, 1995.
[11] Z. Zhou, R. Shinar, A. J. Allison, J. Shinar, *Adv. Funct. Mater.* **2007**, *17*, 3530.
[12] Y. Cai, R. Shinar, Z. Zhou, J. Shinar, *Sens. Actuators B* **2008**, *134*, 727.
[13] D. Ghosh, R. Shinar, V. Dalal, Z. Zhou, J. Shinar, *J. Non Cryst. Solids* **2008**, *354*, 2606.
[14] E. Kraker, A. Haase, B. Lamprecht, G. Jakopic, *Appl. Phys. Lett.* **2008**, *92*, 033302.
[15] *Fiber Optic Chemical Sensors and Biosensors* (Ed: O. S. Wolfbeis), CRC Press, BocaRaton, FL, **1991**.
[16] Y. Amao, *Michrochim. Acta* **2003**, *143*, 1.
[17] G. Li, V. Shrotriya, J. Huang, Y. Yao, T. Moriarty, K. Emery, Y. Yang, *Nat. Mater.* **2005**, *4*, 864.
[18] J. Y. Kim, S. H. Kim, H. H. Lee, K. Lee, W. Ma, X. Gong, A. J. Heeger, *Adv. Mater.* **2006**, *18*, 572.
[19] J. R. Lakowicz, *Principles of Fluorescence Spectroscopy*, Plenum Press, New York **1983**.
[20] M. Sunderberg, O. Inganas, S. Stafstrom, G. Gustafsson, B. Sjogren, *Solid State Commun.* **1989**, *71*, 435.
[21] J. Casado, R. G. Hicks, V. Hernandez, D. J. T. Myles, M. C. R. Delgado, J. T. L. Navarrete, *J. Chem. Phys.* **2003**, *118*, 1912.
[22] Y. W. Goh, Y. F. Lu, Z. M. Rem, T. C. Chong, *Appl. Phys. A: Mater. Sci. Process.* **2003**, *77*, 433.
[23] P. S. O. Patrico, H. D. R. Calado, F. A. C. de Oliveira, A. Righi, B. R. A. Neves, G. G. Silva, L. A. Cury, *J. Phys.: Condens. Matter* **2006**, *18*, 7529.
[24] E. Klimov, W. Li, X. Yang, G. G. Hoffmann, J. Loos, *Macromolecules* **2006**, *39*, 4493.
[25] S. Lee, I. Okura, *Spectrochim. Acta Part A* **1998**, *54*, 91.